
ELECTRICAL AND MAGNETIC
PROPERTIES

Effect of Nb Doping on Thermoelectric Properties of TiNiSn Half-Heusler Alloy Prepared by Microwave Method

Rui-Peng Zhang^a, Lin Bo^a, Xing-Long Wang^a, Wen-Ying Wang^a, Jun-Liang Zhu^a, Ling-Hao Zhao^{a, b},
Min Zuo^a, and De-Gang Zhao^{a, *}

^a School of Materials Science and Engineering, University of Jinan, Jinan, 250022 China

^b Shenzhen Institute of Advanced Electronic Materials, Shenzhen Institute of Advanced Technology,
Chinese Academy of Sciences, Shenzhen, 518055 China

*e-mail: mse_zhaodg@ujn.edu.cn

Received December 4, 2022; revised April 13, 2023; accepted April 19, 2023

Abstract—The inherent high thermal conductivity of TiNiSn half-Heusler (HH) alloy, as well as the long preparation cycle time and high cost of conventional preparation methods limited its commercial application. Herein, Ti_{1-x}Nb_xNiSn half-Heusler alloys with low lattice thermal conductivity were successfully prepared by microwave synthesis combined with rapid hot-pressing sintering, which significantly shortened the preparation cycle and ensured high density of TiNiSn half-Heusler alloys. The effects of Nb substitution at Ti sites on the composition distribution, thermal and electrical transport properties of Ti_{1-x}Nb_xNiSn half-Heusler samples were studied. The maximum *ZT* value of Ti_{0.9}Nb_{0.1}NiSn sample was 0.39 at 725 K due to the increase of power factor (*PF*) and the decrease of lattice thermal conductivity caused by the enhanced phonon scattering, which was about 204% higher than that of undoped TiNiSn.

Keywords: half-Heusler alloy, Ti_{1-x}Nb_xNiSn, microwave synthesis, rapid hot-pressing

DOI: 10.1134/S0031918X22601925

INTRODUCTION

With the rapid development of human society, the demand for energy in industrial production and daily life is gradually increasing. Traditional energy materials are non-renewable and the environmental pollution due to their consumption needs to be solved urgently. Thermoelectric materials, as a new type of environmentally friendly energy material that can directly convert thermal energy into electrical energy, can play a huge role in solving this issue [1]. The performance of thermoelectric materials can be quantified by the dimensionless figure of merit (*ZT*), which can be defined as $ZT = \alpha^2 \sigma T / \kappa$, where α , σ , κ and T are the Seebeck coefficient, electrical conductivity, total thermal conductivity and thermodynamic temperature, respectively [2]. There are two main contributions to the total thermal conductivity, namely lattice thermal conductivity (κ_L) and carrier thermal conductivity (κ_c). An ideal thermoelectric material should have a high power factor ($\alpha^2 \sigma$) to give a high power output from the TE generator and a low thermal conductivity (κ) to maintain a temperature gradient [3]. However, the mutual coupling relationship between α , σ , and κ limits the improvement of thermoelectric figure of merit and the development of thermoelectric materials [4].

The half-Heusler (HH) thermoelectric material crystallized with cubic MgAgAs structure is a ternary compound with the general formula ABX, in which X is the main group element, A and B elements are transition metal elements. The high symmetry of crystal structure endows HH alloys with excellent electrical transport properties, but also makes their thermal transport properties very high, which is detrimental to the improvement of thermoelectric properties. With its high Seebeck coefficient and low resistivity, as well as its advantages of low cost, large quantity, environmental protection and non-toxicity of its constituent elements, MNiSn (M = Zr, Hf, Ti) alloys have become the popular candidates in the HH alloys [1]. But the development of MNiSn alloys is still inevitably limited by their intrinsic high thermal conductivity. Over the past few years, many attempts have been made to optimize the thermoelectric properties of MNiSn alloys, Kim et al. [5] and Sun et al. [6] have been working to tune the carrier concentration by doping Sb on Sn sites. In addition, isoelectronic alloying on the M/Ni sublattice [5, 7–9] or grain refinement in enhancing phonon scattering at boundaries, have been demonstrated the effectiveness in reducing the lattice thermal conductivity [10–12]. However, due to the huge differences in melting points between constituent elements, the adverse effects on pure phase synthesis

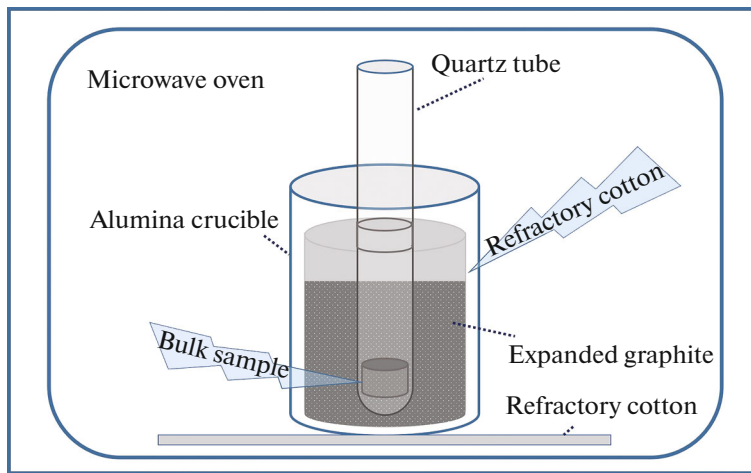


Fig. 1. The process of microwave synthesis.

also restrict the performance optimization and development of industrial production of HH thermoelectric materials [13]. It is worth mentioning that many breakthroughs have been made in the preparation of HH pure phase and the improvement of thermoelectric properties such as the replacement of the traditional preparation method by induction melting, mechanical alloying or other emerging processes [5, 8, 14, 15]. Induction melting and arc melting can avoid the long-time annealing of traditional solid-phase melting to prepare HH pure phase, thereby greatly reducing the preparation cycle and cost. In addition to the above advantages, mechanical alloying and mechanical activation annealing can generate nanocrystalline phase to optimize the thermoelectric figure of merit [15–19]. It is commendable that, as verified by previous reports, microwave-synthesized samples have the advantages of refining grains and improving the uniformity of sample composition. In addition, with the development of recent years, the technique of microwave synthesis has been relatively reliable, and the bulk samples with relatively uniform composition can be synthesized in a few minutes with the help of carbon, silicon carbide and other dielectric materials with high dielectric constant [20–23]. Due to its short preparation cycle, simple process and low manufacturing cost, this synthesis method will attract increasing attention [22, 24–27].

TiNiSn alloy is a kind of medium temperature region half-Heusler thermoelectric material with narrow band gap. With the good compromise between mechanical properties and thermoelectric properties, TiNiSn HH alloys have been extensively studied and indeed have the potential to be excellent thermoelectric materials [28, 29]. In this study, the relatively high-density Nb-doped TiNiSn samples were prepared by microwave synthesis-rapid hot-pressing sintering process, and the effects of Nb-doping on the phase composition, microstructure and thermoelec-

tric properties of TiNiSn alloy were studied in detail. This study is expected to provide useful guidance and reference for the rapid preparation of TiNiSn alloys, and provide a basis for the industrial production of thermoelectric materials.

EXPERIMENTAL

All samples synthesized in this experiment were weighed in accordance with the stoichiometric ratio of Ti powder (99.99%), Ni powder (99.99%), Nb powder (99.99%), Sn powder (99.99%) as initial raw materials, and the total weight of each sample was 6 g. The weighed metal powders and an appropriate amount of anhydrous ethanol were poured into the agate mortar to grind and mix. The dried powders were loaded into a cold-pressing die with a diameter of 12 mm, and were pressed into a round billet under a constant pressure of 10 MPa at room temperature for 5 min. The obtained billet was placed in a clean quartz tube prepared in advance and continuously evacuated until the vacuum was stably maintained below 0.01 Pa. Then the quartz tube was sealed. As shown in Fig. 1, the sealed quartz tube was placed in an alumina crucible laid with refractory wool, and the expanded graphite powder (99.9%, 10–30 μm) was placed inside the crucible as absorbing material. Then the whole quartz tube and crucible were put into microwave equipment for microwave synthesis for 5 min, and the power of microwave equipment was 900 W. The sample synthesized by microwave were mechanically crushed and then placed in a planetary ball mill for ball milling. The speed of the ball mill was set at 300 rpm and the milling time was 5 hours. The obtained powder was loaded into a hot-pressing mould with a diameter of 12 mm for rapid hot-pressing sintering at a pressure of 80 MPa and a temperature of 1123 K for 20 min.

$\text{Ti}_{1-x}\text{Nb}_x\text{NiSn}$ samples were characterized by X-ray diffraction (XRD) using a Rigaku Ultima IV

diffractometer in the 2θ range of 10° – 90° . The surface morphology and microstructure of samples were analyzed by scanning electron microscope (FESEM, JEOL, JXA-8100) and energy dispersive spectrometer. The density of $\text{Ti}_{1-x}\text{Nb}_x\text{NiSn}$ samples was measured by the Archimedes method. The electrical conductivity and Seebeck coefficient of samples can be measured simultaneously by the ZEM-3 system (ULVAC-RIKO) under a low pressure ($\sim 10^2$ Pa) helium atmosphere from room temperature to 725 K. The thermal conductivity (κ) of samples can be calculated according to the formula $\kappa = C_p \lambda d$, here C_p is the specific heat capacity (calculated according to Dulong–Petit law), d is the density, and λ is the thermal diffusion coefficient. The thermal diffusivity coefficient of $\text{Ti}_{1-x}\text{Nb}_x\text{NiSn}$ samples can be determined by the laser flash thermal analyzer (LFA-457, Netzsch). The estimated measurement uncertainty of thermal conductivity, Seebeck coefficient and electrical conductivity was at most 5%.

RESULTS AND DISCUSSION

Figure 2 shows the X-ray diffraction patterns of $\text{Ti}_{1-x}\text{Nb}_x\text{NiSn}$ ($x = 0.01, 0.03, 0.05$ and 0.1) alloys prepared by microwave synthesis and rapid hot-pressing sintering. As shown in Fig. 2, in addition to the existence of TiNiSn HH phase, some impurity phases were indexed as Ti, Sn, Ni_3Sn_4 and TiNi_2Sn Full-Heusler (FH) phase, which may be due to the thermal decomposition of TiNiSn phase at high temperature (1453 K) [30]. It is speculated that Sn was melted after reaching the melting point during rapid hot-pressing sintering and reentered the matrix for reaction. As a result, Sn phase in the synthesized sample was transformed into Ni_3Sn_4 after hot-pressing sintering. And samples with higher Nb content may be more prone to form the secondary phases. The similar phenomenon was also observed in the $\text{TiNi}_{1+x}\text{Sn}$ system [31]. The presence of these metallic phases inevitably contributed to the increase of electrical conductivity of sample [17, 32]. In addition, in the enlarged XRD pattern of the sintered bulk, it can be found that with the increase of Nb substitution, the (220) diffraction peak shifted slightly to the low-angle direction, which was due to the fact that the ionic radius of Nb (69 pm) is much larger than that of Ti (60.5 pm).

As shown in Table 1, the relative densities of $\text{Ti}_{1-x}\text{Nb}_x\text{NiSn}$ alloys were above 95%, which were measured over more than three measurements. The relatively high density is usually positively correlated with electrical transport properties of thermoelectric materials [33]. These interesting results indicated that HH thermoelectric materials with high density can be successfully prepared by microwave synthesis combined with rapid hot-pressing sintering.

The SEM images of cross-sectional morphology of the $\text{Ti}_{0.9}\text{Nb}_{0.1}\text{NiSn}$ sample at different magnifications were analyzed by scanning electron microscope. It can

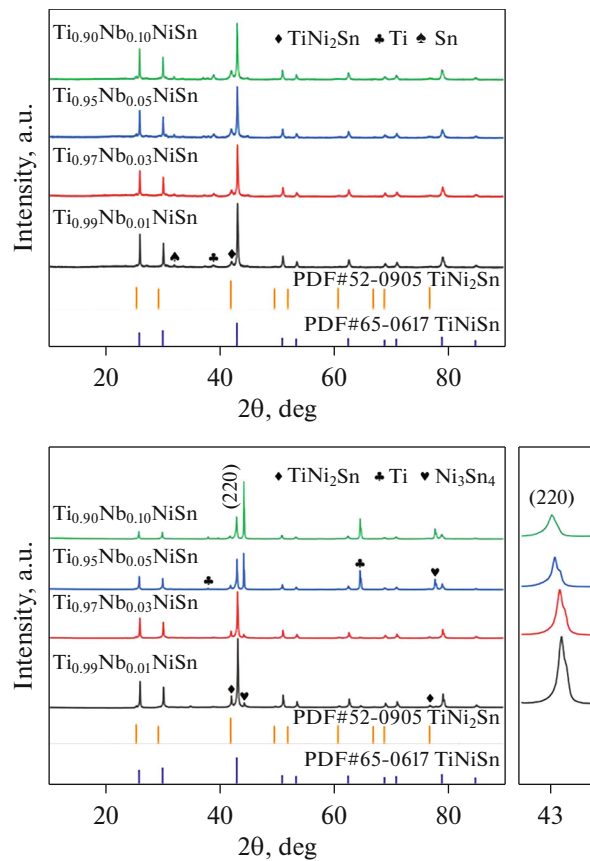


Fig. 2. XRD patterns of $\text{Ti}_{1-x}\text{Nb}_x\text{NiSn}$ ($x = 0.01, 0.03, 0.05$ and 0.1) alloys. (a) Powder samples after microwave synthesis, and (b) bulk samples after rapid hot-pressing sintering.

be seen in Fig. 3 that in addition to the existence of small grains among large grains, there were still some submicron/nano pores. Although the existence of these submicron/nano pores would adversely affect the electrical transport of thermoelectric materials, it can also avoid the excessive thermal conductivity [34]. In order to determine the phase composition of different grains in Fig. 3, energy dispersive spectroscopy (EDS) compositional point analysis and EDS compo-

Table 1. The density (d), relative density (η), carrier concentration (n) and carrier mobility (μ) of $\text{Ti}_{1-x}\text{Nb}_x\text{NiSn}$ ($x = 0, 0.01, 0.03, 0.05$ and 0.1) alloys

Composition	d , g/cm ³	η , %	n , 10 ²¹ cm ⁻³	μ , cm ² V ⁻¹ s ⁻¹
TiNiSn	7.025	98.25	1.529	2.393
$\text{Ti}_{0.99}\text{Nb}_{0.01}\text{NiSn}$	6.861	95.96	1.778	1.968
$\text{Ti}_{0.97}\text{Nb}_{0.03}\text{NiSn}$	6.924	96.84	2.491	2.889
$\text{Ti}_{0.95}\text{Nb}_{0.05}\text{NiSn}$	6.990	97.76	3.237	3.321
$\text{Ti}_{0.9}\text{Nb}_{0.1}\text{NiSn}$	7.026	98.27	4.324	3.765

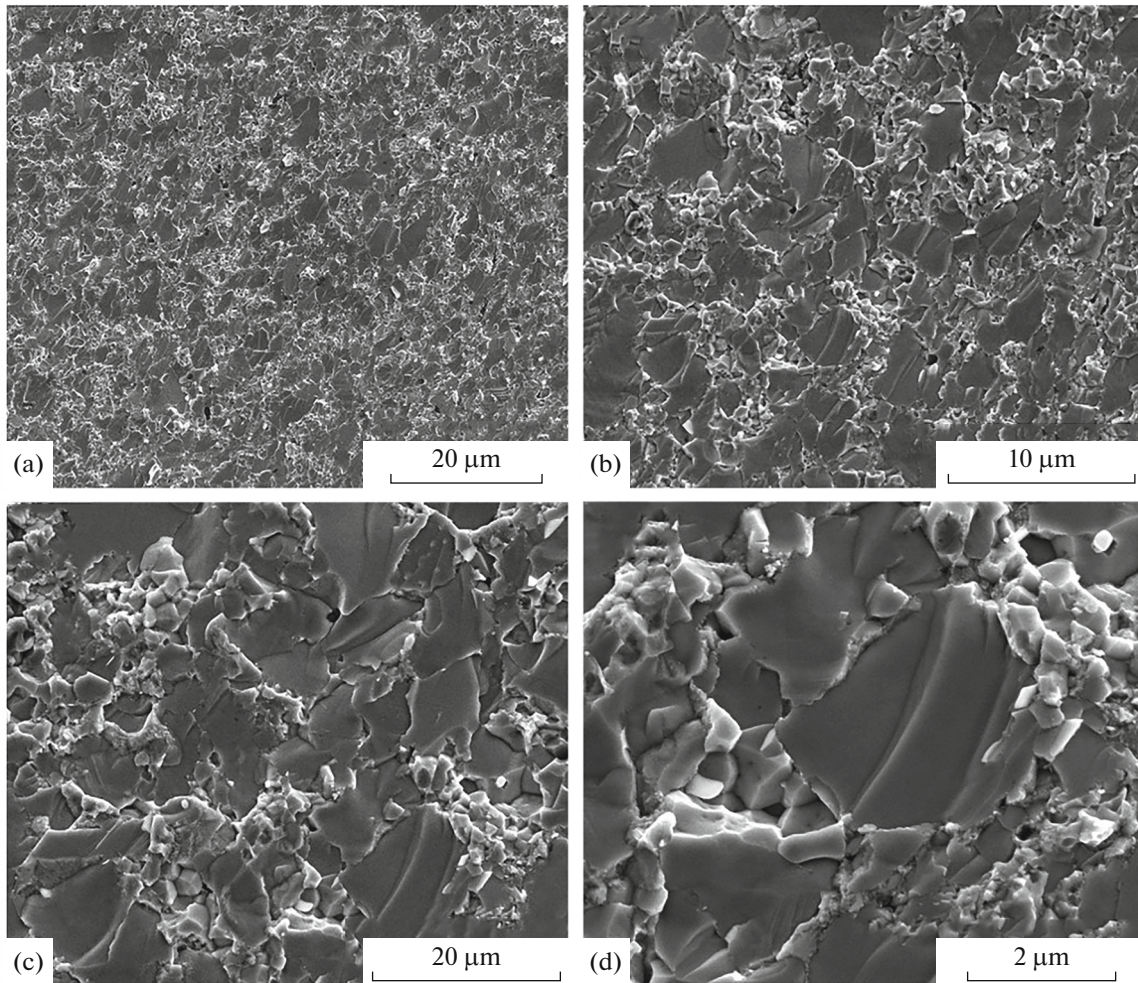


Fig. 3. SEM images of cross-sectional morphology of $\text{Ti}_{0.9}\text{Nb}_{0.1}\text{NiSn}$ alloy at different magnifications: (a) 2000, (b) 5000, (c) 10000, and (d) 20000.

sitional mapping were carried out on the basis of back-scattering electron image analysis for the $\text{Ti}_{0.9}\text{Nb}_{0.1}\text{NiSn}$ sample (Figs. 4 and 5). As shown in Fig. 4, the mapping results of $\text{Ti}_{0.9}\text{Nb}_{0.1}\text{NiSn}$ sample showed that all the constituent elements had slight element segregation, which verified the appearance of the second phases in the XRD results. This was due to the heteroatom incorporation of Nb and the thermal decomposition of the TiNiSn HH phase at high temperature. Combining the EDS mapping and point analysis results, it can be speculated that the white area (point 1) and the area of yellow dotted circle in Fig. 4 should be a mixture of TiNi_2Sn and Ni_3Sn_4 . Moreover, the black area (point 2) contained the Ti-rich phase, and the gray area (point 3) corresponded the TiNiSn HH matrix phase.

Figure 6a shows electrical conductivity of $\text{Ti}_{1-x}\text{Nb}_x\text{NiSn}$ ($x = 0, 0.01, 0.03, 0.05$ and 0.1) alloys as a function of temperature. As shown in Fig. 6a, the electrical conductivity of all samples except

$\text{Ti}_{0.99}\text{Nb}_{0.01}\text{NiSn}$ alloy was higher than that of the undoped TiNiSn alloy. More electrons can be introduced to participate in electrical transport due to the incorporation of Nb, suggesting that the conductivity of $\text{Ti}_{1-x}\text{Nb}_x\text{NiSn}$ alloys should generally be higher than that of TiNiSn sample [35, 36]. However, the conductivity of $\text{Ti}_{0.99}\text{Nb}_{0.01}\text{NiSn}$ sample was lower than that of TiNiSn alloy. This was mainly due to the lower relative density of $\text{Ti}_{0.99}\text{Nb}_{0.01}\text{NiSn}$ than that of other samples. In addition, the presence of metallic second phases also affected the electrical transport performance. It can be seen from Fig. 6a that the electrical conductivity of $\text{Ti}_{1-x}\text{Nb}_x\text{NiSn}$ alloys ($x > 0.03$) decreased with temperature, which was manifested as metallic characteristic. This phenomenon was also observed in the ZrNiSn system, which resulted from the change of the energy band structure caused by doping and the overlapping of the energy bands [37, 38].

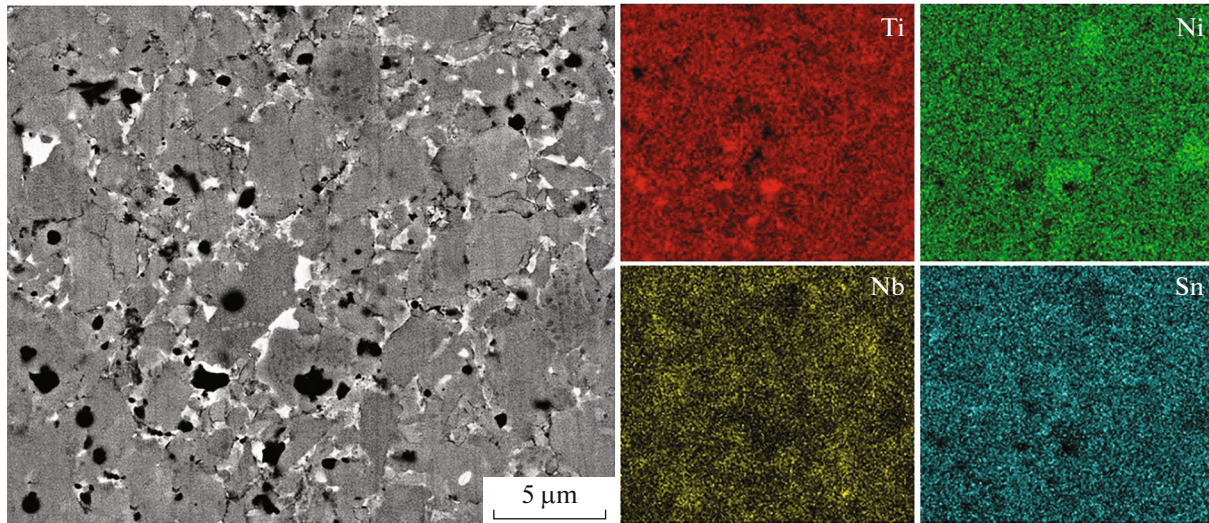


Fig. 4. BSE image and EDS compositional mapping of the polished surface of $\text{Ti}_{0.9}\text{Nb}_{0.1}\text{NiSn}$ alloy.

As shown in Fig. 6b, the Seebeck coefficient of $\text{Ti}_{1-x}\text{Nb}_x\text{NiSn}$ alloys was negative over the entire temperature range, indicating that samples exhibited *n*-type semiconductor properties. For degenerate semiconductor, the Seebeck coefficient α is usually related to the carrier concentration that can be expressed by the Mott equation [4]:

$$\alpha = \frac{8\pi^2 k_B^2}{3eh^2} m^* T \left(\frac{\pi}{3n} \right)^{\frac{2}{3}},$$

where k_B , e , h , T , m^* , n are Boltzmann constant, elementary charge, Planck constant, absolute temperature, density of states (DOS) effective mass and carrier concentration, respectively. The absolute values of α of all Nb-doped samples were larger than that of TiNiSn , indicating that the incorporation of Nb was beneficial to the increase of α , which could be due to the increase of effective mass. The maximum α increased from $85 \mu\text{V K}^{-1}$ for TiNiSn to $129 \mu\text{V K}^{-1}$ for $\text{Ti}_{0.97}\text{Nb}_{0.03}\text{NiSn}$ sample at 725 K. However, the α of $\text{Ti}_{0.95}\text{Nb}_{0.05}\text{NiSn}$ and $\text{Ti}_{0.9}\text{Nb}_{0.1}\text{NiSn}$ samples decreased compared with that of the $\text{Ti}_{0.97}\text{Nb}_{0.03}\text{NiSn}$, which might be related to the excessive carrier concentration (Table 1) caused by heavy Nb doping. Moreover, the α in this work is significantly lower than that of previous work ($235 \mu\text{V K}^{-1}$) [39], which was due to the additional increase of electrical conductivity caused by the secondary phases.

Figure 6c shows the power factor as a function of temperature for the $\text{Ti}_{1-x}\text{Nb}_x\text{NiSn}$ alloys calculated from the electrical conductivity and the Seebeck coefficient. It can be seen from Fig. 6c that the power factor of $\text{Ti}_{0.99}\text{Nb}_{0.01}\text{NiSn}$ was higher than that of $\text{Ti}_{1-x}\text{Nb}_x\text{NiSn}$ alloys due to the increased absolute value of the Seebeck coefficient. Especially, the *PF* of $\text{Ti}_{0.97}\text{Nb}_{0.03}\text{NiSn}$ and $\text{Ti}_{0.9}\text{Nb}_{0.1}\text{NiSn}$ was much higher than that of TiNiSn . The maximum *PF* of

$\text{Ti}_{0.9}\text{Nb}_{0.1}\text{NiSn}$ was $24.59 \mu\text{W cm}^{-1} \text{K}^{-2}$, which was 226% higher than that of TiNiSn ($7.53 \mu\text{W cm}^{-1} \text{K}^{-2}$).

Figures 7a–7c are the curves of total thermal conductivity (κ), electronic thermal conductivity (κ_e), and lattice thermal conductivity (κ_L) of $\text{Ti}_{1-x}\text{Nb}_x\text{NiSn}$ alloys as a function of temperature, respectively. For the Nb-doped samples, the fluctuation of the total thermal conductivity in the temperature range was not obvious, which meant that the device made of the $\text{Ti}_{1-x}\text{Nb}_x\text{NiSn}$ alloys better stability in the operating state. The electronic thermal conductivity (κ_e) was calculated by Wiedemann–Franz law ($\kappa_e = L\sigma T$), the Lorentz constant L was taken as $2.45 \times 10^{-8} \text{ W Ohm K}^{-2}$. The electronic thermal conductivity increased with the increasing Nb content, which was consistent with the variation trend of electrical conductivity. The reason for this was that more carriers carried more energy for thermal transport, resulting in higher electronic thermal conductivity [40].

The lattice thermal conductivity (κ_L) obtained by subtracting electronic thermal conductivity from total thermal conductivity included the contribution of bipolar effect to thermal conductivity [41]. It can be seen from Fig. 7c that Nb substitution at Ti sites had a significant effect on reducing the lattice thermal conductivity of the $\text{Ti}_{1-x}\text{Nb}_x\text{NiSn}$ alloys. The greater the Nb content, the better the reduction effect of thermal conductivity. Compared with Ti atom, Nb atom has larger relative atomic mass and larger ionic radius. Consequently, besides introducing point defects in the lattice, the stress field and mass field wave scattering were introduced into the $\text{Ti}_{1-x}\text{Nb}_x\text{NiSn}$ alloys when the Ti was substituted by Nb atom, which was conducive to decreasing the lattice thermal conductivity. The main reason was that the existence of point defects and nano/submicron pores led to the reduction of mean

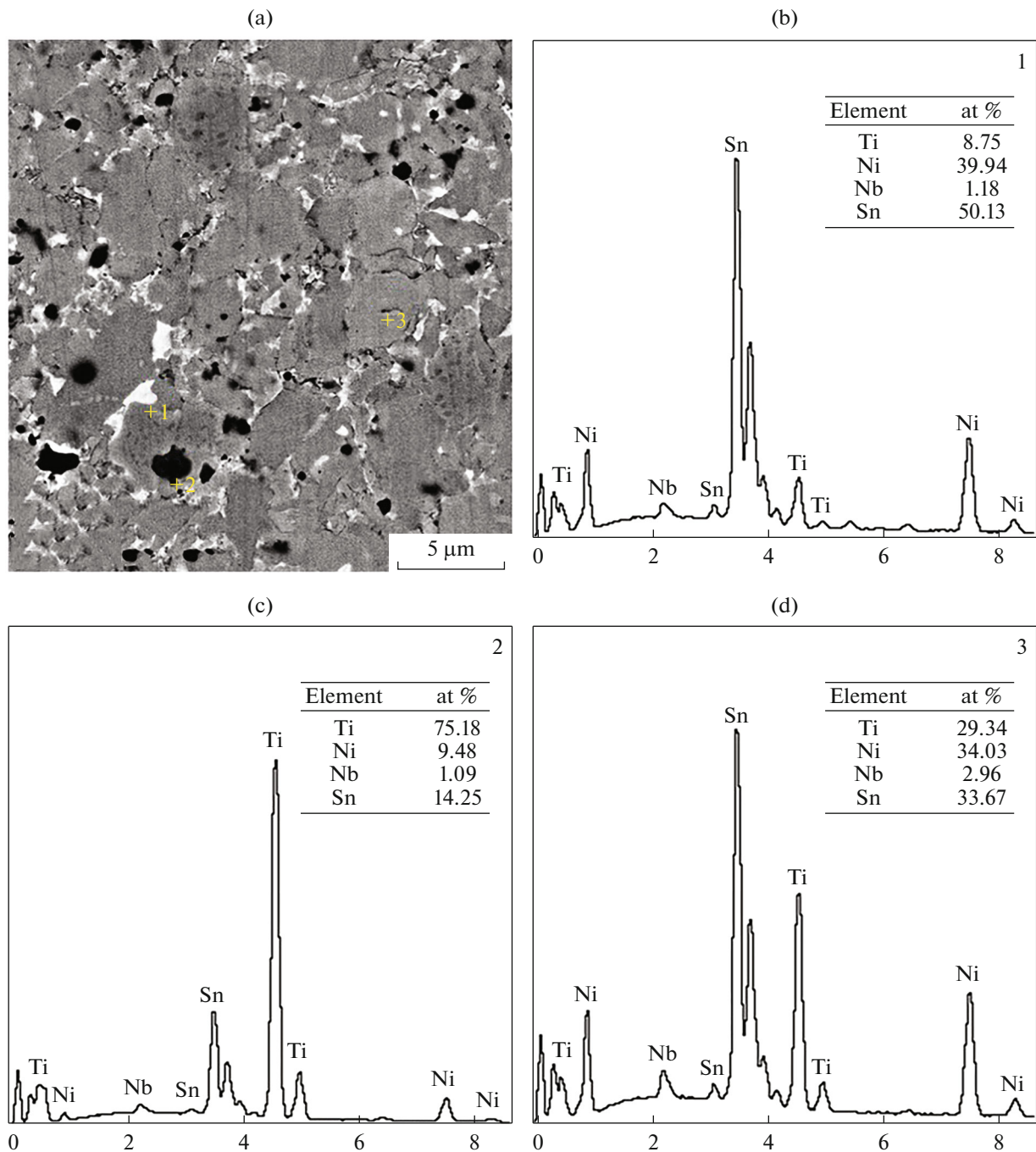


Fig. 5. BSE image and EDS compositional point analysis of the polished surface of $\text{Ti}_{0.9}\text{Nb}_{0.1}\text{NiSn}$ alloy. (a) BSE image, (b) EDS of point 1, (c) EDS of point 2, and (d) EDS of point 3.

free path of phonons, which in turn enhanced the scattering of phonons, thereby reducing the κ_L . In addition, the effectiveness of interfacial scattering between the HH phase and secondary phases for reducing the lattice thermal conductivity had also been demonstrated [9, 14, 42–45]. For most HH materials, the simple crystal structures lead to the relatively high lattice thermal conductivity. The lattice thermal conductivity of the $\text{Ti}_{0.9}\text{Nb}_{0.1}\text{NiSn}$ sample in

this study was reduced to about $1 \text{ W m}^{-1} \text{ K}^{-1}$ at high temperature, which was much lower than that of TiNiSn . It proved that it is feasible to reduce the thermal conductivity by incorporating Nb into TiNiSn .

The temperature-dependent figure of merit (ZT) for $\text{Ti}_{1-x}\text{Nb}_x\text{NiSn}$ ($x = 0, 0.01, 0.03, 0.05$ and 0.1) alloys is shown in Fig. 8. It can be seen that although the electronic thermal conductivity was greatly increased, the ZT of $\text{Ti}_{1-x}\text{Nb}_x\text{NiSn}$ samples increased

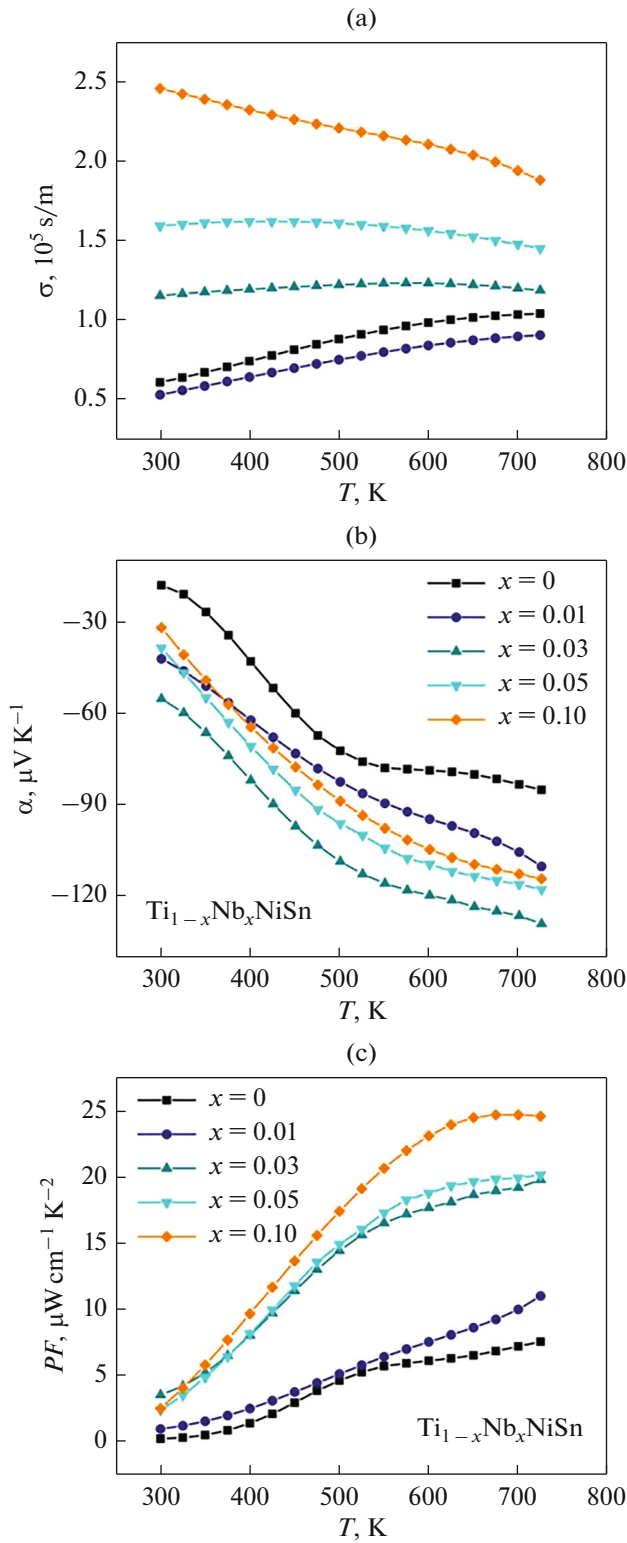


Fig. 6. The electrical properties of $\text{Ti}_{1-x}\text{Nb}_x\text{NiSn}$ ($x = 0, 0.01, 0.03, 0.05$ and 0.1) alloys. (a) Electrical conductivity, (b) Seebeck coefficient, and (c) power factor.

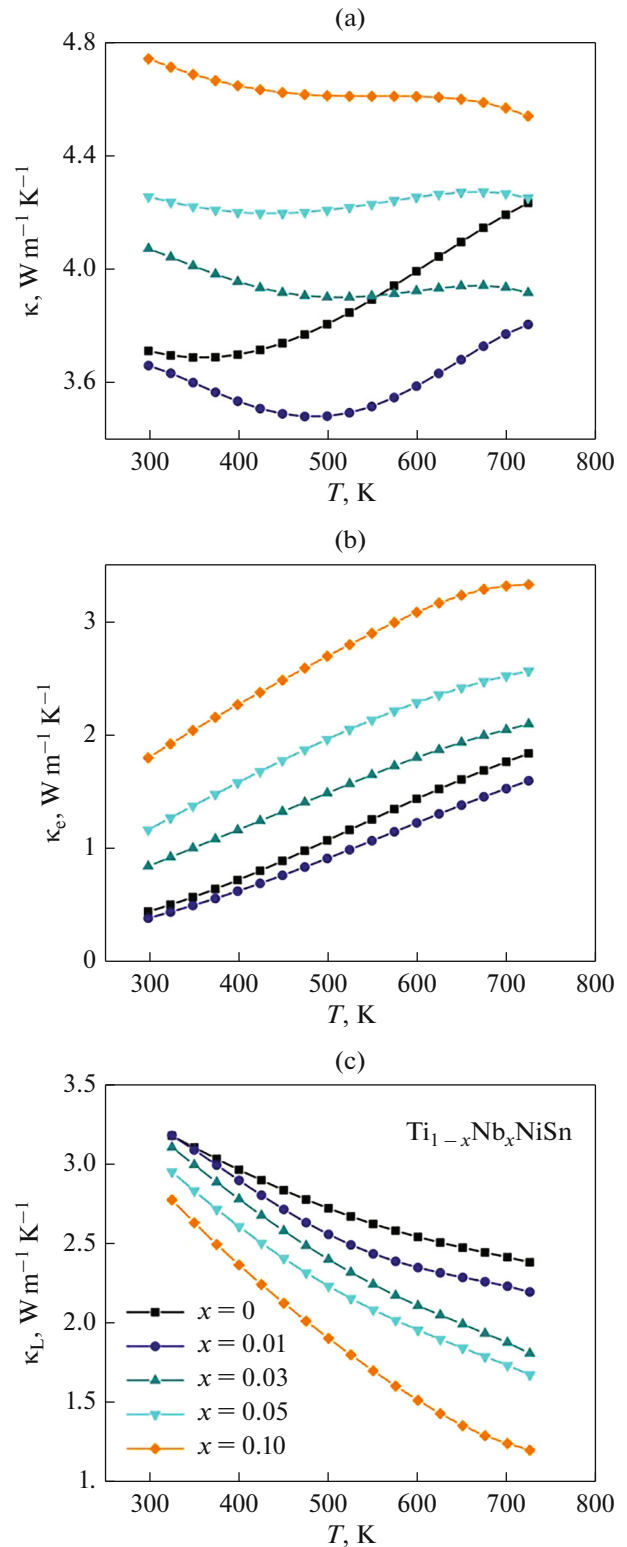


Fig. 7. The thermal properties of $\text{Ti}_{1-x}\text{Nb}_x\text{NiSn}$ ($x = 0, 0.01, 0.03, 0.05$ and 0.1) alloys. (a) Total thermal conductivity, (b) electronic thermal conductivity, and (c) lattice thermal conductivity.

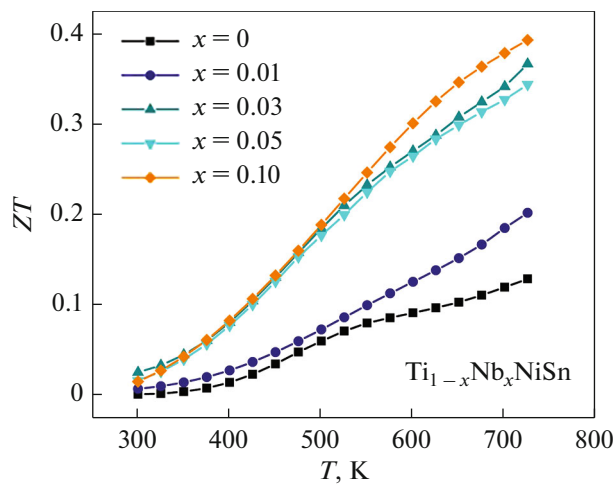


Fig. 8. Thermoelectric figure of merit ZT of $Ti_{1-x}Nb_xNiSn$ ($x = 0, 0.01, 0.03, 0.05,$ and 0.1) alloys as a function of temperature.

compared with that of $TiNiSn$ samples due to the significant decrease in the lattice thermal conductivity. The average ZT of $Ti_{0.9}Nb_{0.1}NiSn$ sample in the temperature range was 0.21, which was even higher than the maximum value of 0.13 for $TiNiSn$ at 725 K. However, the maximum ZT of 0.39 for $Ti_{0.9}Nb_{0.1}NiSn$ at 725 K is still lower than the 0.57 for $Ti_{0.98}Nb_{0.02}NiSn$ reported by Muta et al. [39], which may be attributed to the fact that the optimization of thermal conductivity in this work is not sufficient to bridge the gap in power factor caused by the small Seebeck coefficient.

CONCLUSIONS

In this study, the $Ti_{1-x}Nb_xNiSn$ ($x = 0-0.1$) alloys with high density were successfully prepared by microwave synthesis combined with ball milling and rapid hot-pressing sintering process. With the incorporation of different amounts of Nb into $TiNiSn$, the electrical conductivity of $Ti_{1-x}Nb_xNiSn$ alloys increased markedly. At the same time, the absolute value of Seebeck coefficient also increased significantly due to the Nb substitution at Ti sites. In addition, the lattice thermal conductivity of $Ti_{1-x}Nb_xNiSn$ alloys decreased due to the presence of point defects leading to mass/stress fields fluctuations. Although the electronic thermal conductivity of $Ti_{1-x}Nb_xNiSn$ alloys was partially increased, it was not enough to offset the positive effect of thermoelectric performance caused by the reduction of lattice thermal conductivity and the increase of power factor. Consequently, the ZT of all $Ti_{1-x}Nb_xNiSn$ samples increased compared with that of $TiNiSn$ alloy.

ACKNOWLEDGMENTS

The authors would like to thank Yanzhong Pei Group at Tongji University for the partial measurement of TE properties.

FUNDING

This work was supported by the National Natural Science Foundation of China (grant no. 51772132), Shandong Province Higher Educational Youth Innovative Science and Technology Program (grant no. 2019KJA018) and the leader of scientific research studio program of Jinan (grant no. 2021GXRC082).

CONFLICT OF INTEREST

The authors of this work declare that they have no conflicts of interest.

REFERENCES

1. C. Uher, J. Yang, S. Hu, D. Morelli, and G. Meisner, "Transport properties of pure and doped $MNiSn$ ($M = Zr, Hf$)," *Phys. Rev. B* **59**, 8615–8621 (1999). <https://doi.org/10.1103/physrevb.59.8615>
2. C. Gayner and K. K. Kar, "Recent advances in thermoelectric materials," *Prog. Mater. Sci.* **83**, 330–382 (2016). <https://doi.org/10.1016/j.pmatsci.2016.07.002>
3. G. Tan, L.-D. Zhao, and M. G. Kanatzidis, "Rationally designing high-performance bulk thermoelectric materials," *Chem. Rev.* **116**, 12123–12149 (2016). <https://doi.org/10.1021/acs.chemrev.6b00255>
4. G. J. Snyder and E. S. Toberer, "Complex thermoelectric materials," *Nat. Mater.* **7**, 105–114 (2008). <https://doi.org/10.1038/nmat2090>
5. S.-W. Kim, Yo. Kimura, and Yo. Mishima, "High temperature thermoelectric properties of $TiNiSn$ -based half-Heusler compounds," *Intermetallics* **15**, 349–356 (2007). <https://doi.org/10.1016/j.intermet.2006.08.008>
6. Yi. Sun, W. Qiu, L. Zhao, H. He, L. Yang, L. Chen, H. Deng, X. Shi, and J. Tang, "Defects engineering driven high power factor of $ZrNiSn$ -based half-Heusler thermoelectric materials," *Chem. Phys. Lett.* **755**, 137770 (2020). <https://doi.org/10.1016/j.cplett.2020.137770>
7. N. Jia, J. Cao, X. Tan, J. Dong, H. Liu, C. Tan, J. Xu, Q. Yan, X. Loh, and A. Suwardi, "Thermoelectric materials and transport physics," *Mater. Today Phys.* **21**, 100519 (2021). <https://doi.org/10.1016/j.mtphys.2021.100519>
8. K. Kurosaki, T. Maekawa, H. Muta, and S. Yamanaka, "Effect of spark plasma sintering temperature on thermoelectric properties of $(Ti, Zr, Hf)NiSn$ half-Heusler compounds," *J. Alloys Compd.* **397**, 296–299 (2005). <https://doi.org/10.1016/j.jallcom.2005.01.028>
9. R. Yan, R. Xie, W. Xie, C. Shen, W. Li, B. Balke, S. Yoon, H. Zhang, and A. Weidenkaff, "Effects of doping Ni on the microstructures and thermoelectric properties of co-excessive $NbCoSn$ half-Heusler com-

- pounds,” *ACS Appl. Mater. Interfaces* **13**, 34533–34542 (2021).
<https://doi.org/10.1021/acsami.1c08127>
10. C. Hu, K. Xia, C. Fu, X. Zhao, and T. Zhu, “Carrier grain boundary scattering in thermoelectric materials,” *Energy Environ. Sci.* **15**, 1406–1422 (2022).
<https://doi.org/10.1039/d1ee03802h>
 11. T. Ghosh, M. Dutta, D. Sarkar, and K. Biswas, “Insights into low thermal conductivity in inorganic materials for thermoelectrics,” *J. Am. Chem. Soc.* **144**, 10099–10118 (2022).
<https://doi.org/10.1021/jacs.2c02017>
 12. X. Zhang, S. Li, B. Zou, P. Xu, Yi. Song, B. Xu, Yi. Wang, G. Tang, and S. Yang, “Significant enhancement in thermoelectric properties of half-Heusler compound TiNiSn by grain boundary engineering,” *J. Alloys Compd.* **901**, 163686 (2022).
<https://doi.org/10.1016/j.jallcom.2022.163686>
 13. A. Karati, M. Nagini, S. Ghosh, R. Shabadi, K. Pradeep, R. Mallik, B. Murty, and U. Varadaraju, “Ti₂NiCoSnSb—A new half-Heusler type high-entropy alloy showing simultaneous increase in Seebeck coefficient and electrical conductivity for thermoelectric applications,” *Sci. Rep.* **9**, 5331 (2019).
<https://doi.org/10.1038/s41598-019-41818-6>
 14. J. P. Makongo, D. K. Misra, X. Zhou, A. Pant, M. R. Shabetai, X. Su, C. Uher, K. L. Stokes, and P. F. Poudeu, “Simultaneous large enhancements in thermopower and electrical conductivity of bulk nanostructured half-Heusler alloys,” *J. Am. Chem. Soc.* **133**, 18843–18852 (2011).
<https://doi.org/10.1021/ja206491j>
 15. Ya. Gelbstein, N. Tal, A. Yarmek, Yo. Rosenberg, M. Dariel, S. Ouardi, B. Balke, C. Felser, and M. Köhne, “Thermoelectric properties of spark plasma sintered composites based on TiNiSn half-Heusler alloys,” *J. Mater. Res.* **26**, 1919–1924 (2011).
<https://doi.org/10.1557/jmr.2011.107>
 16. B. Balke, J. Barth, M. Schwall, G. H. Fecher, and C. Felser, “An alternative approach to improve the thermoelectric properties of half-Heusler compounds,” *J. Electron. Mater.* **40**, 702–706 (2011).
<https://doi.org/10.1007/s11664-011-1517-0>
 17. H. Xie, H. Wang, C. Fu, Yi. Liu, G. J. Snyder, X. Zhao, and T. Zhu, “The intrinsic disorder related alloy scattering in ZrNiSn half-Heusler thermoelectric materials,” *Sci. Rep.* **4**, 6888 (2014).
<https://doi.org/10.1038/srep06888>
 18. A. Karati, S. Mukherjee, R. C. Mallik, R. Shabadi, B. Murty, and U. Varadaraju, “Simultaneous increase in thermopower and electrical conductivity through Ta-doping and nanostructuring in half-Heusler TiNiSn alloys,” *Materialia* **7**, 100410 (2019).
<https://doi.org/10.1016/j.mtla.2019.100410>
 19. A. Karati and B. Murty, “Synthesis of nanocrystalline half-Heusler TiNiSn by mechanically activated annealing,” *Mater. Lett.* **205**, 114–117 (2017).
<https://doi.org/10.1016/j.matlet.2017.06.068>
 20. J. W. Lekse, T. J. Stagger, and J. A. Aitken, “Microwave metallurgy: Synthesis of intermetallic compounds via microwave irradiation,” *Chem. Mater.* **19**, 3601–3603 (2007).
<https://doi.org/10.1021/cm0707410>
 21. K. Biswas, S. Muir, and M. A. Subramanian, “Rapid microwave synthesis of indium filled skutterudites: An energy efficient route to high performance thermoelectric materials,” *Mater. Res. Bull.* **46**, 2288–2290 (2011).
<https://doi.org/10.1016/j.materresbull.2011.08.058>
 22. D. Baghurst, A. Chippindale, and D. M. P. Mingos, “Microwave syntheses for superconducting ceramics,” *Nature* **332**, 311 (1988).
<https://doi.org/10.1038/332311a0>
 23. Yo. Wang, W. Wang, H. Zhao, L. Bo, L. Wang, F. Li, M. Zuo, and D. Zhao, “Rapid microwave synthesis of Cu₂Se thermoelectric material with high conductivity,” *Funct. Mater. Lett.* **14**, 2151008 (2021).
<https://doi.org/10.1142/s1793604721510085>
 24. A. Agostino, P. Volpe, M. Castiglioni, and M. Truccato, “Microwave synthesis of MgB₂ superconductor,” *Mater. Res. Innovations* **8**, 75–77 (2004).
<https://doi.org/10.1080/14328917.2004.11784833>
 25. W. L. E. Wong, S. Karthik, and M. Gupta, “Development of high performance Mg–Al₂O₃ composites containing Al₂O₃ in submicron length scale using microwave assisted rapid sintering,” *Mater. Sci. Technol.* **21**, 1063–1070 (2005).
<https://doi.org/10.1179/174328405x51758>
 26. L. Wang, R. Zhang, L. Bo, F. Li, Ya. Hou, M. Zuo, and D. Zhao, “Effects of different pressing process on the microstructure and thermoelectric properties of TiNiSn_{1-x}Tex half-Heusler alloy prepared by microwave method,” *JOM* **74**, 4250–4257 (2022).
<https://doi.org/10.1007/s11837-022-05464-0>
 27. L. Bo, R. Zhang, H. Zhao, Ya. Hou, X. Wang, J. Zhu, L. Zhao, M. Zuo, and D. Zhao, “Achieving high thermoelectric properties of Cu₂Se via lattice softening and phonon scattering mechanism,” *ACS Appl. Energy Mater.* **5**, 6453–6461 (2022).
<https://doi.org/10.1021/acsaem.2c00949>
 28. F. Aliev, N. Brandt, V. Moshchalkov, V. Kozyrkov, R. Skolozdra, and A. Belogorokhov, “Gap at the Fermi level in the intermetallic vacancy system RBiSn (R = Ti, Zr, Hf),” *Z. Phys. B Condens. Matter* **75**, 167–171 (1989).
<https://doi.org/10.1007/bf01307996>
 29. F. Aliev, V. Kozyrkov, V. Moshchalkov, R. Skolozdra, and K. Durczewski, “Narrow band in the intermetallic compounds MNiSn (M = Ti, Zr, Hf),” *Z. Phys. B Condens. Matter* **80**, 353–357 (1990).
<https://doi.org/10.1007/bf01323516>
 30. D.-Yo. Jung, K. Kurosaki, Ch.-E. Kim, H. Muta, and Sh. Yamanaka, “Thermal expansion and melting temperature of the half-Heusler compounds: MNiSn (M = Ti, Zr, Hf),” *J. Alloys Compd.* **489**, 328–331 (2010).
<https://doi.org/10.1016/j.jallcom.2009.09.139>
 31. C. S. Birkel, J. E. Douglas, B. R. Lettiere, G. Seward, N. Verma, Yi. Zhang, T. M. Pollock, R. Seshadri, and G. D. Stucky, “Improving the thermoelectric properties of half-Heusler TiNiSn through inclusion of a second full-Heusler phase: Microwave preparation and spark plasma sintering of TiNi_{1+x}Sn,” *Phys. Chem. Chem. Phys.* **15**, 6990 (2013).
<https://doi.org/10.1039/c3cp50918d>
 32. F. Aversano, M. Palumbo, A. Ferrario, S. Boldrini, C. Fanciulli, M. Baricco, and A. Castellero, “Role of secondary phases and thermal cycling on thermoelec-

- tric properties of TiNiSn half-Heusler alloy prepared by different processing routes,” *Intermetallics* **127**, 106988 (2020).
<https://doi.org/10.1016/j.intermet.2020.106988>
33. K. Biswas, J. He, I. D. Blum, Ch.-I. Wu, T. P. Hogan, D. N. Seidman, V. P. Dravid, and M. G. Kanatzidis, “High-performance bulk thermoelectrics with all-scale hierarchical architectures,” *Nature* **489**, 414–418 (2012).
<https://doi.org/10.1038/nature11439>
 34. Yi-X. Zhang, Q. Lou, Zh.-H. Ge, Sh.-W. Gu, J.-X. Yang, J. Guo, Yu-K. Zhu, Yi. Zhou, X.-H. Yu, J. Feng, and J. He, “Excellent thermoelectric properties and stability realized in copper sulfides based composites via complex nanostructuring,” *Acta Mater.* **233**, 117972 (2022).
<https://doi.org/10.1016/j.actamat.2022.117972>
 35. L. Huang, R. He, S. Chen, H. Zhang, K. Dahal, H. Zhou, H. Wang, Q. Zhang, and Z. Ren, “A new *n*-type half-Heusler thermoelectric material NbCoSb,” *Mater. Res. Bull.* **70**, 773–778 (2015).
<https://doi.org/10.1016/j.materresbull.2015.06.022>
 36. A. Karati, V. Hariharan, S. Ghosh, A. Prasad, M. Nagini, K. Guruvidyathri, R. C. Mallik, R. Shabadi, L. Bichler, B. Murty, and U. Varadaraju, “Thermoelectric properties of half-Heusler high-entropy $\text{Ti}_2\text{NiCoSn}_{1-x}\text{Sb}_{1+x}$ ($x = 0.5, 1$) alloys with VEC > 18,” *Scr. Mater.* **186**, 375–380 (2020).
<https://doi.org/10.1016/j.scriptamat.2020.04.036>
 37. G. Mesaritis, I. Ioannou, A. Delimitis, E. Hatzikraniotis, Y. Gelbstein, and T. Kyratsi, “*n*-type (Zr, Ti)NiSn half Heusler materials via mechanical alloying: Structure, Sb-doping and thermoelectric properties,” *J. Phys. Chem. Solids* **167**, 110735 (2022).
<https://doi.org/10.1016/j.jpcs.2022.110735>
 38. J. Chen, H. Yang, C. Liu, J. Liang, L. Miao, Z. Zhang, P. Liu, K. Yoshida, C. Chen, Q. Zhang, Q. Zhou, Yu. Liao, P. Wang, Z. Li, and B. Peng, “Strategy of extra zr doping on the enhancement of thermoelectric performance for TiZr_xNiSn synthesized by a modified solid-state reaction,” *ACS Appl. Mater. Interfaces* **13**, 48801–48809 (2021).
<https://doi.org/10.1021/acsami.1c14723>
 39. H. Muta, T. Kanemitsu, K. Kurosaki, and S. Yamana-ka, “High-temperature thermoelectric properties of Nb-doped MNiSn ($M = \text{Ti, Zr}$) half-Heusler compound,” *J. Alloys Compd.* **469**, 50–55 (2009).
<https://doi.org/10.1016/j.jallcom.2008.02.041>
 40. R.-F. Wang, S. Li, W.-H. Xue, C. Chen, Yu-M. Wang, X.-J. Liu, and Q. Zhang, “Enhanced thermoelectric performance of *n*-type TiCoSb half-Heusler by Ta doping and Hf alloying,” *Rare Met.* **40**, 40–47 (2021).
<https://doi.org/10.1007/s12598-020-01569-0>
 41. G. Uğur, A. K. Kushwaha, M. Güler, Z. Charifi, Ş. Uğur, E. Güler, and H. Baaziz, “Electronic structure, optical and vibrational properties of $\text{Ti}_2\text{FeNiSb}_2$ and $\text{Ti}_2\text{Ni}_2\text{InSb}$ double half Heusler alloys,” *Mater. Sci. Semicond. Process.* **123**, 105531 (2021).
<https://doi.org/10.1016/j.mssp.2020.105531>
 42. K. Chen, C. Nuttall, E. Stefanaki, K. Placha, R. Tuley, K. Simpson, J.-W. G. Bos, and M. Reece, “Fast synthesis of *n*-type half-Heusler TiNiSn thermoelectric material,” *Scr. Mater.* **191**, 71–75 (2021).
<https://doi.org/10.1016/j.scriptamat.2020.09.010>
 43. H. B. Kang, B. Poudel, W. Li, H. Lee, U. Saparamadu, A. Nozariasbmarz, M. G. Kang, A. Gupta, J. J. Heremans, and S. Priya, “Decoupled phononic-electronic transport in multi-phase *n*-type half-Heusler nanocomposites enabling efficient high temperature power generation,” *Mater. Today* **36**, 63–72 (2020).
<https://doi.org/10.1016/j.mattod.2020.01.002>
 44. I. Ioannou, P. S. Ioannou, A. Delimitis, Ya. Gelbstein, I. J. Giapintzakis, and T. Kyratsi, “High thermoelectric performance of *p*-type half-Heusler (Hf, Ti)Co(Sb, Sn) solid solutions fabricated by mechanical alloying,” *J. Alloys Compd.* **858**, 158330 (2021).
<https://doi.org/10.1016/j.jallcom.2020.158330>
 45. V. I. Okulov, A. T. Lonchakov, and V. V. Marchenkov, “Semiconductor-like behavior of electric transport in Fe–V–Al-based metallic alloys and their uncommon magnetic properties,” *Phys. Met. Metallogr.* **119**, 1325–1328 (2018).
<https://doi.org/10.1134/s0031918x18130240>

Publisher’s Note. Pleiades Publishing remains neutral with regard to jurisdictional claims in published maps and institutional affiliations.